INTERGRANULAR AND INTERPHASE BOUNDARIES IN MATERIALS

Structure, phase composition, and microhardness of carbon steels after high-pressure torsion

Andrei A. Mazilkin · Boris B. Straumal ·
Svetlana G. Protasova · Sergei V. Dobatkin ·
Brigitte Baretzky

Abstract The phase composition, mechanical properties, and microstructure of binary Fe–C alloys with various carbon concentrations (0.25, 0.45, 0.6, 1.3, 1.5, and 1.7 wt.%) were studied by transmission electron microscopy, X-ray diffraction analysis, and microhardness measurements. The investigations were carried out for three states of the material, namely for as-cast, annealed (725 °C) and deformed by high-pressure torsion (HPT) samples. The grain size after HPT is in the nanometer range. Only Fe_3C (cementite) and α-Fe remain in the alloys after HPT. The residual austenite disappears and phase composition closely approaches the equilibrium corresponding to the temperature and pressure of HPT. Analysis of the microhardness behavior revealed that hardening of the deformed alloys takes place due to the grain refinement and dispersoid mechanism.

Introduction

Manufacturing materials with a very small grain size in the nanometer range is an important way of improving their mechanical properties [1]. Such nanograined alloys are considerably stronger than their coarse-grained counterparts and at the same time they retain reasonable ductility. Different variants of severe plastic deformation (SPD) are very promising techniques for obtaining nanograined metals. Such SPD techniques like equal channel angular pressing (ECAP) and high-pressure torsion (HPT) do not induce changes in the material geometry compared to the conventional deformation processes like rolling or wire drawing. Apparently the SPD grain refinement from millimeter or micrometer to the nanometer range automatically leads to the strengthening of a material. However, it has been demonstrated recently that SPD along with the grain refinement may simultaneously result in the material softening [2]. This means that the processes of structural changes during SPD are very complicated and have not yet been fully understood. Comprehensive investigation of nanograined polycrystals is important especially for two- and multicomponent systems, which are of the most importance for the technological use. The Fe–C system belongs to the alloys of crucial importance for structural and functional applications. The aim of this work is to study the structure and mechanical properties of Fe–C alloys in the broad interval of a carbon concentration in an as-cast state, after HPT deformation and after long annealing in the $\alpha + Fe_3C$ region of the Fe–C phase diagram.

A. A. Mazilkin (✉) · B. B. Straumal · S. G. Protasova
Institute of Solid State Physics, Russian Academy of Sciences,
Chernogolovka 142432, Russia
e-mail: mazilkin@issp.ac.ru

B. B. Straumal · B. Baretzky
Max-Planck-Institut für Metallforschung, Heisenbergstrasse 3,
70569 Stuttgart, Germany

S. V. Dobatkin
A.A. Baikov Institute of Metallurgy and Materials Science,
Russian Academy of Sciences, Leninsky prosp. 49, 119991
Moscow, Russia

Experimental

Iron–carbon alloys with carbon concentrations of 0.25, 0.45, 0.60, 1.3, 1.5, and 1.7 wt.% were prepared from high-purity 5N Fe and C by vacuum induction melting in the form of cylindrical 12 mm diameter ingots. The 2 mm

thick discs were cut from the cast ingots in order to investigate the as-cast state. Discs of 0.4 mm thickness and 12 mm diameter were subjected to HPT in a Bridgman anvil-type unit at room temperature and pressure at 5 GPa (5 torsions, shear strain was about 6). Samples for structural investigations were cut from the HPT-deformed discs at a distance of about 3 mm from the sample center (i.e., in the middle of the HPT disc radius). Some of the cast alloys with 0.25, 0.60, 1.3, and 1.7 wt.% C were additionally annealed during 950 h at 725 °C (i.e., slightly below the temperature of eutectoid transformation) in order to achieve a structure corresponding to the equilibrium Fe–C phase diagram. Light microscopy (LM), transmission electron microscopy (TEM), and X-ray diffraction analysis (XRDA) were engaged to perform structural investigations of the alloys. Mechanical properties of the alloys were characterized by microhardness measurements on a standard facility with a load of 200 g. The value of microhardness was evaluated as a result of 10 measurements for each experimental point.

Results and discussion

X-ray measurements

The phase state of the alloys after different treatment was characterized by the XRDA technique. It was established that ferrite and cementite were the main structural elements in all as-cast alloys. Also the residual austenite was detected with a volume fraction of about 10%. Both the HPT deformation and the long annealing at 725 °C (i.e., below the eutectoid temperature) resulted in the structure equilibration: the residual austenite disappeared and the phase composition of the alloys corresponded to the equilibrium phase diagram at room temperature [3]. It was also reported [4] that the lattice parameter of the α-Fe solid solution in the samples after HPT corresponded to about 0.01 wt.% C, i.e., to the solubility at room temperature [5]. The lattice parameter of the (Fe) solid solution in the

as-cast alloys does not differ from that in the HPT state more than 10^{-4} nm. Magnetization measurements [4] also support the fact that the phase composition of the alloys is very close to the equilibrium one. In other words, HPT does not lead to the formation of supersaturated carbon solid solution in α-Fe. It looks that ball milling is quite different from this point of view: the formation of supersaturated carbon solid solution was reported by Ohsaki et al. [6]. Most probably, the ball milling influences the free surfaces of milled particles and in certain point is similar to the ion implantation. In the early work, Korznikov et al. [7] observed the disappearance of cementite peaks from XRD spectra and supposed that, similar to the ball milling, SPD leads to the formation of supersaturated carbon solid solution in α-Fe. However, the later careful measurements demonstrated that the very fine cementite particles and carbon segregation layers in the ferrite GBs form during SPD, but not the oversaturated carbon solid solution in α-Fe [8–10]. Therefore, the early hypothesis that SPD can lead to the formation of supersaturated solid solution in steels [7] was not supported by the later experiments [8–10].

Microstructure investigations with LM and TEM

As-cast alloys

Figure 1 illustrates the microstructures of the hypo- and hypereutectoid as-cast alloys obtained by light microscopy. In the alloy with 0.25 wt.% C (Fig. 1a), the following structural components are present: (i) the ferrite grains, (ii) the austenite grains transformed into ferrite + austenite mixture during cooling through the ferrite + austenite region of the Fe–C phase diagram; (iii) initial austenite plates transformed into perlite or troostite. The amount of the primary ferrite decreases with increasing carbon content. The microstructures of hypereutectoid alloys (the alloy with 1.3 wt.% C as shown in Fig. 1b) are similar to each other, but differ from those of

Fig. 1 Light micrographs of as-cast Fe–C alloys with 0.25 (**a**) and 1.3 (**b**) wt.% C. The austenite is transformed into troostite and appears grey in all micrographs. In Fig. 1a ferrite appears white. In Fig. 1b cementite appears white
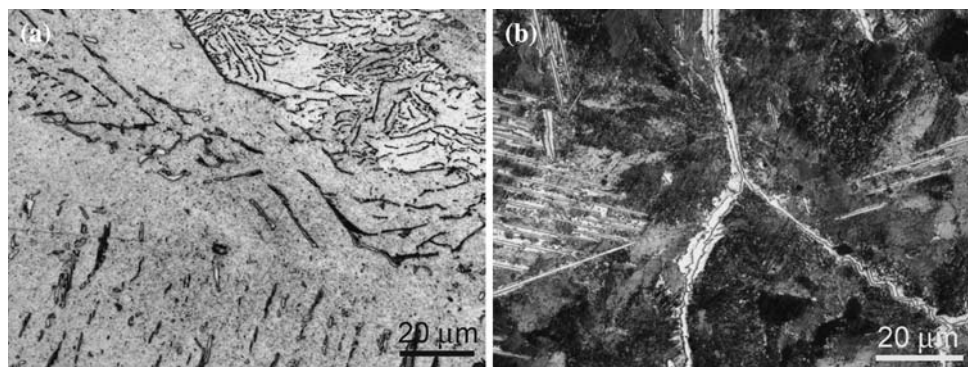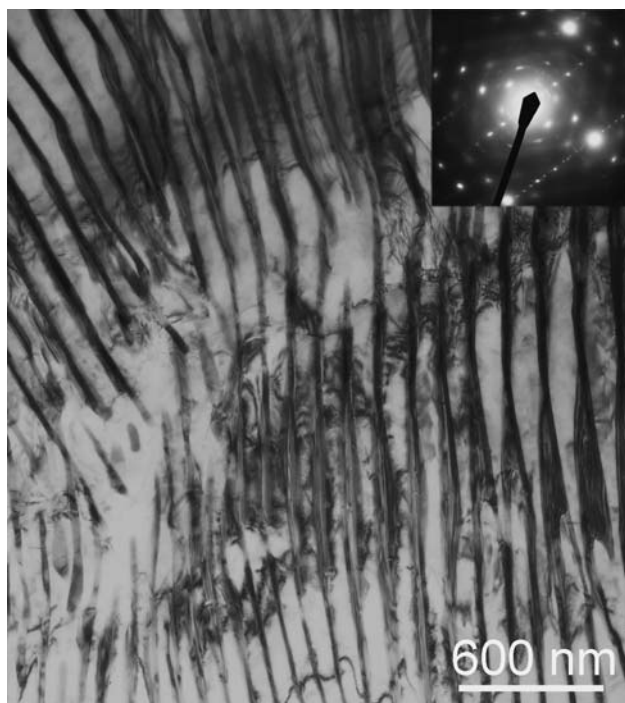
Fig. 2 Bright field TEM image of the coarse grained as-cast Fe–1.3 wt.% C alloy and respective electron diffraction pattern as an insert. Fine cementite lamellae appear dark inside the bright ferrite grains

hypoeutectoid alloys. They contain the initial austenite grains transformed into troostite which appear grey. Grain boundaries between former austenite grains are covered by the cementite layers.

In Fig. 2, the bright field TEM image of the coarse grained as-cast Fe–1.3% C alloy and respective electron diffraction pattern are shown. Transformed austenite grains contain troostite lamellar colonies with interlammellar spacing of 100–400 nm. The presence of ferrite and cementite in the structure is supported by the electron diffraction pattern and illustrates also the presence of small amounts of Hägg carbide in the as-cast alloys. TEM of the as-cast alloys with 0.25, 0.45, 0.60, 1.3, and 1.5 wt.% C revealed the presence of ferrite and cementite in all studied

alloys. Only the amount of these phases is different in various alloys in conformity with Fe–C phase diagram [3]. According to the light microscopy and TEM, the grain size of ferrite (in hypoeutectoid alloys), residual and transformed austenite (in all alloys) in studied as-cast alloys scattered from 200 to 700 μm.

Alloys annealed at 725 °C

Figure 3 illustrates the LM microstructures of the Fe–C alloys with 0.25 and 1.3 wt.% C additionally annealed at 725 °C for 950 h in order to achieve the equilibrium α-Fe + Fe_3C structure. After long annealing, the structures of hypoeutectoid and hypereutectoid alloys became very similar. All the samples contain very coarse ferrite and cementite grains. Only the amount of cementite is different, which increases with increasing carbon content, according to the Fe–C phase diagram [3].

Alloys after HPT

Figure 4 shows the bright field (Fig. 4a) and the dark field (Fig. 4b) TEM micrographs of the Fe–0.25 wt.% C alloy. The electron diffraction pattern (Fig. 4c) contains only α-Fe and Fe_3C spots. The TEM micrographs and electron diffraction patterns of other Fe alloys after HPT are very similar to those shown in Fig. 4. The ferrite grain size after HPT is about 100 nm. It increases slightly with increasing carbon content. The grains are not equiaxial; they are slightly elongated parallel to the direction of the deformation. The cementite grain size in all studied alloys is about 30 nm, which confirms estimations made using the X-rays line broadening. Their shape is more equiaxial than that of the ferrite grains and they are rather uniformly distributed over the specimen. The spacing between cementite particles decreases with increasing carbon content. It is about 50–100 nm in Fe–0.25 wt.% C alloy and about 10–50 nm in the Fe–1.7 wt.% C alloys.

Fig. 3 Light micrographs of the Fe–C alloys with 0.25 wt.% C (**a**) and 1.3 wt.% C (**b**) annealed at 735 °C, 950 h (below the eutectoid temperature)
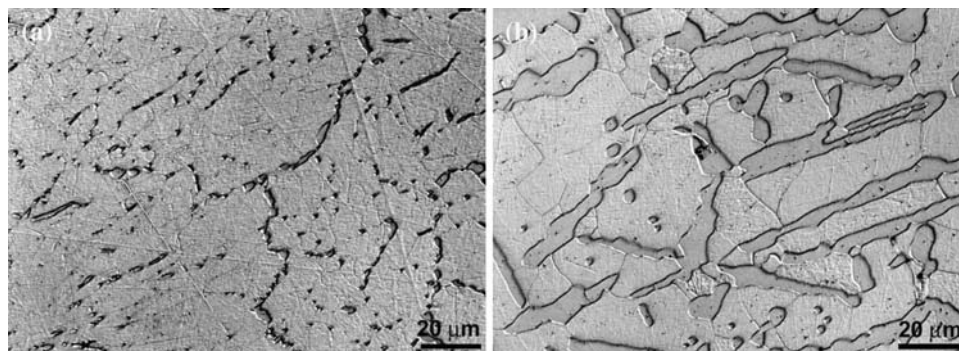
Fig. 4 Bright (**a**) and dark (**b**) field TEM micrographs of the same location of Fe–0.25 wt.% C alloy after HTP; (**c**) electron diffraction pattern revealing α-Fe and Fe₃C spots
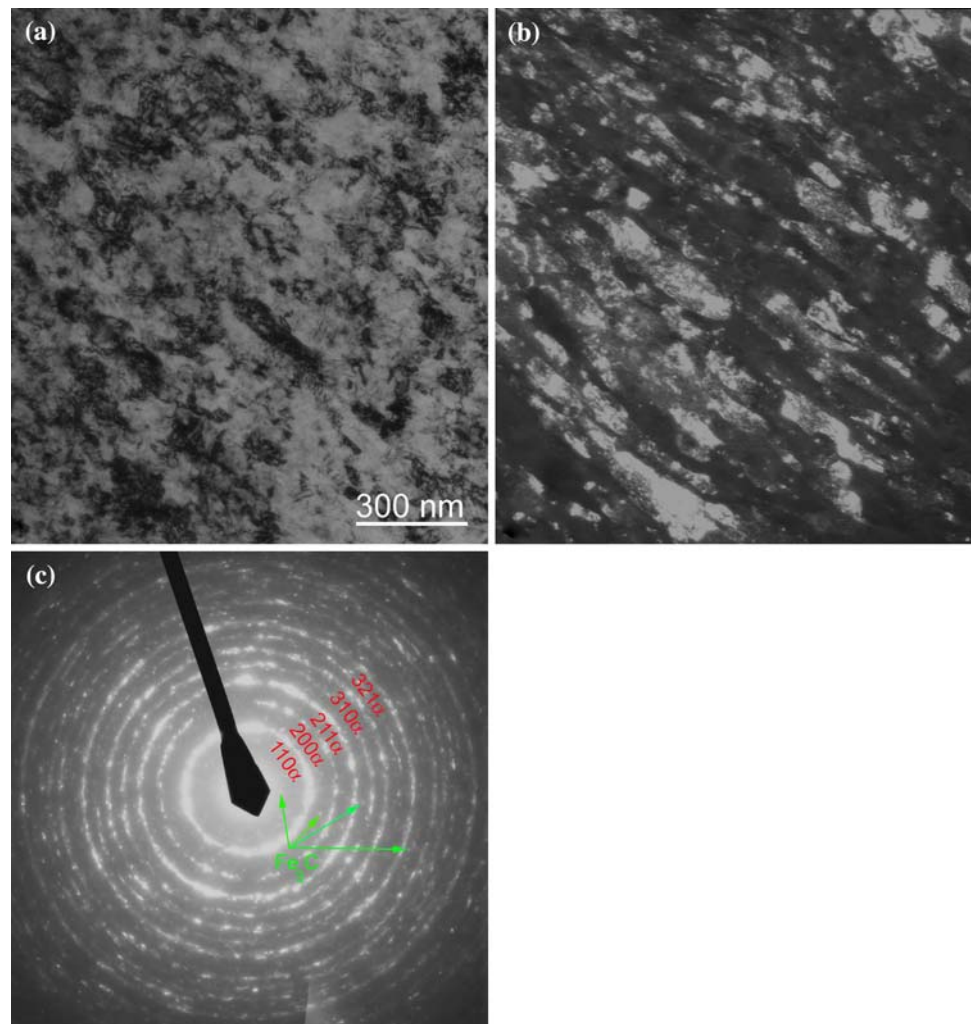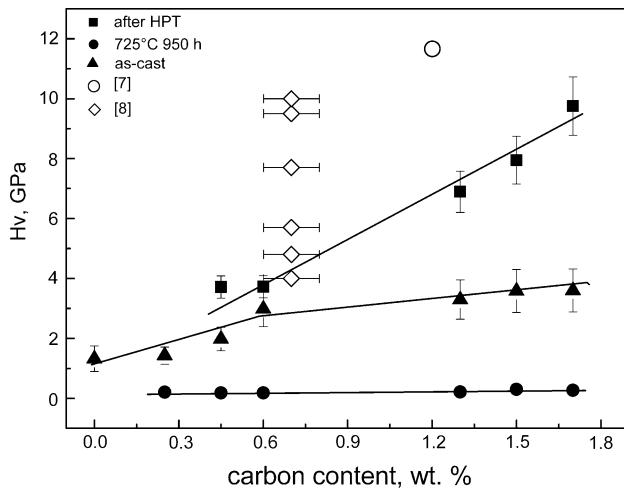

Microhardness

Results of the microhardness measurements of the Fe–C alloys with different carbon concentrations and in different structural states are presented in Fig. 5. In all as-cast alloys, the hardness grows with increasing carbon content. The lattice parameter of the as-cast alloys does not differ from that in the equilibrium state. Therefore, the increase of the microhardness cannot be attributed to the solid solution hardening as in the previously studied Al–Zn alloys [11]. The microhardness growth increase seems to be due to the dispersoid hardening. Dispersoid hardening appears since the dispersed particles form the obstacles for the dislocation glide [12]. The morphology of cementite grains in hypo- and hypereutectoid as-cast alloys is rather different. It is reflected in the different slope of the *Hv* dependence on carbon concentration for as-cast alloys (Fig. 5). After HPT the morphology of ferrite and cementite grains is similar below and above 0.8 wt.% C. As a result, all *Hv* values for HPT alloys fit well to unique straight line.

In the annealed samples, the microhardness substantially decreases in respect to the as-cast state, which is explained by: (i) complete equilibration of the composition of all phases, (ii) decrease of the dislocation density, and (iii) drastic increase of the cementite grain size and disappearance of the cementite hardening precipitates. This can be easily observed in the LM images (Fig. 3), where the precipitates are rather spherical than needle-shaped.

Microhardness of HPT alloys increases with increasing carbon content, but this is not associated with the change in their lattice parameter. This means that the hardening takes place due to the dispersoid and Hall–Petch mechanisms [13, 14]. The Hall–Petch hardening is attributed to the difference in orientation of the slip systems in two neighboring grains. This causes difficulties in the slip transfer across the grain boundaries and the resulting dislocation pile-ups hinder further deformation.

The data obtained for iron–carbon alloys after the SPD by Korznikov et al. [7] and Ivanisenko et al. [8] have been also inserted in the Fig. 5. The nanograined state of the UIC 860V pearlitic steel [8], containing 0.6–0.8% C,

Fig. 5 Microhardness of the Fe–C alloys with different carbon concentrations in as-cast state, after HPT and after annealing at 725 °C, 950 h. The results for the steel Fe – 1.2% C – 0.22% Mn – 0.25% Zn – 0.01% S – 0.025% P – 0.2% Mg – 0.2% Cu (concentrations in wt.%) after HPT at 10 GPa with true deformation $e = 7$ [7] and UIC 860V pearlitic steel (0.6–0.8% C, 0.8–1.3% Mn, 0.1–0.5% Si, 0.04% S and 0.04% P) after HPT at 7 GPa, and 0, 1.5, 2, 3, 5 and 7 anvil rotations [8] are also presented

0.8–1.3% Mn, 0.1–0.5% Si, 0.04% S, and 0.04% P, was also produced by the HPT technique but the applied pressure was 7 GPa. The hardness steadily increases by increasing the degree of deformation, expressed in the number of anvil rotations. To acquire a deformation close to our samples with a microhardness value of about 9.5 GPa, which is somewhat higher than that presented in this article, a higher pressure was applied. In [7], the steel Fe–1.2 wt.% C–0.22 wt.% Mn–0.25 wt.% Zn–0.01 wt.% S–0.025 wt.% P–0.2 wt.% Mg–0.2 wt.% Cu was HPT deformed at 10 GPa with true deformation $e = 7$. Both deformation and pressure were higher than in our case. This is probably the reason why the microhardness was also higher. Another reason for the increased hardness could be the presence of additional alloying elements in the steels studied in [7, 8].

Hall–Petch mechanism can be responsible for the hardening of HPT alloys in compared to the as-cast ones, since HPT deformation of the as-cast alloys leads to the grain refinement. However, the grain size does not change much with increasing carbon content both for the as-cast and HPT alloys. Therefore, it can be attributed to the dispersoid mechanism proposed by Mott and Nabarro [12]. According to [12], the hardening ΔHv can be written as $\Delta Hv = a \, L_d^{-3}$, where L_d is the mean distance between obstacles and a is the constant depending on the shear modulus, Burgers vector, number and radius of dislocation loops remaining around each obstacle. In [15], we measured saturation magnetization and coercivity of the same Fe–C alloys. These data allowed us to estimate the mean

distance L between pinning points for the domain walls movement based on the Kersten model [16]. In this model, it is assumed that the domain walls move by the magnetization through the array of pinning points. If the external magnetic field increases, the pinned domain wall bends first and then jumps to the next neighboring pair of pining points, similar as dislocation does by deformation. We suppose that obstacles for the dislocation glide and pinning points for the domain walls movement have the same nature and plot in Fig. 6, the microhardness against L^{-3}. It is clearly seen from Fig. 6 that the obtained dependence is distinctly divided into three parts. The first part corresponds to the long annealed samples, the second part corresponds to the as-cast state and the third part corresponds to the samples after HPT deformation. The dependence for the as-cast alloys can be easily explained by changes in the microstructure from low-carbon to high-carbon alloys. The value of L can be identified as the distance between minor cementite platelets or particles. By increasing the carbon content, the amount of cementite increases and the distance between Fe_3C platelets or particles decreases which is perfectly reflected by the dependence. For all HPT alloys L is lower compared to the as-cast alloys. TEM revealed that the mean distance between cementite particles decreases with increasing carbon content. This fact is illustrated by the behavior of Mott–Nabarro dependence in Fig. 6. Different slope of the as-cast and HPT samples can be attributed to the different morphology of obstacles: cementite platelets in as-cast alloys (Fig. 2) and spherical particles in HPT alloys (Fig. 4).
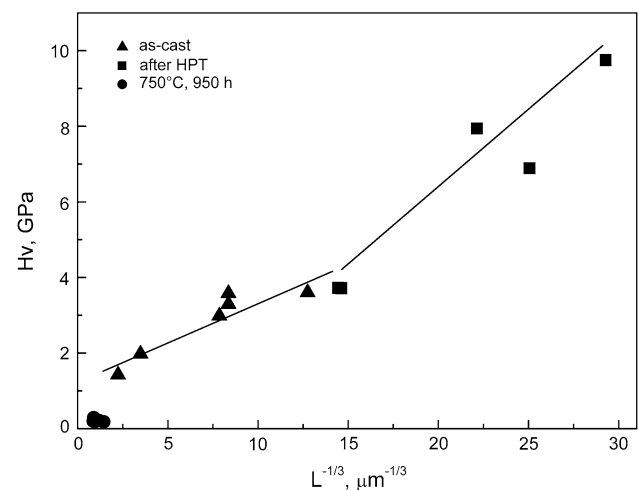
Fig. 6 Dependence of the microhardness Hv on the cubic root of the distance between the pinning points L for the domain wall movement in the studied alloys

Conclusions

Severe plastic deformation leads to a drastic increase in hardness for both hypoeutectoid and hypereutectoid Fe–C alloys. The hardening of alloys after HPT can be attributed to the influence of numerous interphase and grain boundaries in the nanograined structure formed after HPT (Hall–Petch mechanism). The hardiness increase of as-cast and HPT alloys with increasing carbon content can be attributed to the dispersoid hardening (Mott–Nabarro mechanism).

References

1. Valiev R (2004) Nat Mater 3:511; (2002) Nature 419:887
2. Xu Ch, Furukawa M, Horita Z, Langdon TG (2005) Acta Mater 53:749
3. Massalski TB (ed) (1990) Binary alloy phase diagrams. ASM International, Materials Park, pp 147–149
4. Straumal BB, Mazilkin AA, Protasova SG, Dobatkin SV, Rodin AO, Baretzky B, Goll D, Schütz G (2007) Acta Mater (to be published)
5. Hasebe M, Ohtani H, Nishizawa T (1985) Met Trans A 16:913
6. Ohsaki S, Hono K, Hidaka H, Takaki S (2005) Scripta Mater 52:271
7. Korznikov AV, Ivanisenko YuV, Laptionok DV, Safarov IM, Pilyugin VP, Valiev RZ (1994) NanoStruct Mater 4:159
8. Ivanisenko Yu, Lojkovski W, Valiev RZ, Fecht H-J (2003) Acta Mater 51:5555
9. Ivanisenko Yu, MacLaren I, Sauvage X, Valiev RZ, Fecht H-J (2006) Acta Mater 54:1659
10. Sauvage X, Ivanisenko Yu (2007) J Mater Sci 42:1615
11. Mazilkin AA, Straumal BB, Rabkin E, Baretzky B, Enders S, Protasova SG, Kogtenkova OA, Valiev RZ (2006) Acta Mater 54:3933
12. Mott NF, Nabarro FRN (1940) Proc Phys Soc 52:86
13. Hall EO (1951) Proc Phys Soc B 64:747
14. Petch NJ (1953) J Iron Steel Inst 173:25
15. Protasova SG, Straumal BB, Dobatkin SV, Goll D, Schütz G, Baretzky B, Mazilkin AA, Nekrasov AN (2007) J Mater Sci (this issue)
16. Kersten M (1956) Z Angew Phys 7:313; 8:382; 8:496